

Mechanical Property Enhancement of Ti-6Al-4V by Multilayer Thin Solid Film Ti/TiO₂ Nanotubular Array Coating for Biomedical Application

ERFAN ZALNEZHAD, SAEID BARADARAN, A.R. BUSHROA
and AHMED A.D. SARHAN

With the intention of improving the mechanical properties of Ti-6Al-4V, samples were first coated with pure titanium using the physical vapor deposition (PVD) magnetron sputtering technique. The Taguchi optimization method was used to attain a higher coating on substrate adhesion. Second, pure titanium-coated samples with higher adhesion were anodized to generate TiO₂ nanotubes. Next, the TiO₂-coated specimens were heat treated at annealing temperatures of 753.15 K and 923.15 K (480 °C and 650 °C). The XRD results indicate that the varying heat treatment temperatures produced different phases, namely, anatase [753.15 K (480 °C)] and rutile [923.15 K (650 °C)]. Finally, the coated samples' mechanical properties (surface hardness, adhesion, and fretting fatigue life) were investigated. The fretting fatigue lives of TiO₂-coated specimens at 753.15 K and 923.15 K (480 °C and 650 °C) annealing temperatures were significantly enhanced compared to uncoated samples at low and high cyclic fatigue. The results also indicate that TiO₂-coated samples heat treated at an annealing temperature of 753.15 K (480 °C) (anatase phase) are more suitable for increasing fretting fatigue life at high cyclic fatigue (HCF), while at low cyclic fatigue, the annealing temperature of 923.15 K (650 °C) seemed to be more appropriate. The fretting fatigue life enhancement of thin-film TiO₂ nanotubular array-coated Ti-6Al-4V is due to the ceramic nature of TiO₂ which produces a hard surface as well as a lower coefficient of friction of the TiO₂ nanotube surface that decreases the fretting between contacting components, namely, the sample and friction pad surfaces.

DOI: 10.1007/s11661-013-2043-x

© The Minerals, Metals & Materials Society and ASM International 2013

I. INTRODUCTION

TITANIUM and its alloys exhibit the most suitable characteristics for biomedical applications owing to their high biocompatibility, specific strength, and corrosion resistance.^[1] They are currently utilized as metallic structural biomaterials in implants such as artificial hip joints and dental roots; they are mainly used in implants that replace hard tissue. They are also required to possess high strength and long fatigue life, that is, high fatigue strength. Nowadays, a low Young's modulus equivalent to that of cortical bone is simultaneously required in order to inhibit bone absorption.^[2] Porous titanium and its alloys have also been developed for the fabrication of titanium alloys with low Young's modulus. In addition, functionalities such as superelasticity

and shape memory characteristics are currently essential for titanium alloys used in biomedical applications. The mechanism of superelastic behavior of some titanium alloys in biomedical applications is still unknown.^[3] Wear loss occurs, for example, between the stem and bone, along with loosening. There is a possibility of fretting fatigue taking place in the contact area of two bodies, for example, between the bone plate and screw. Therefore, the wear and fretting fatigue characteristics are also very important factors for titanium alloys employed in biomedicine.^[1,2] Young's modulus as well as tensile strength, ductility, fatigue life, fretting fatigue life, wear properties, functionalities, *etc.*, should be controlled in such a manner that they are at levels suitable for structural biomaterials in implants that replace hard tissue. These factors may be collectively referred to as mechanical biocompatibilities in a broader sense.

Several sorts of coatings exist with the potential to develop the mechanical properties of metallic materials. Some methods such as chemical vapor deposition (CVD), hard anodizing (HA), plasma spray, physical vapor deposition (PVD), electrophoretic, dipping and electrochemical deposition, pulsed laser deposition, ion beam dynamic mixing, and ion beam deposition have been explored with respect to improving thin coatings of metals.^[4–11] However, a number of these techniques have limitations like poor adhesion, microcracks, phase

ERFAN ZALNEZHAD, is with the Department of Mechanical Engineering, Faculty of Engineering, University of Malaya, 50630 Kuala Lumpur, Malaysia, and also with the Faculty of Engineering, Islamic Azad University, Chalous Branch, Iran. Contact e-mail: erfanz@um.edu.my SAEID BARADARAN, Ph.D. Student, and A.R. BUSHROA, Senior Lecturer, are with the Department of Mechanical Engineering, Faculty of Engineering, University of Malaya. AHMED A.D. SARHAN, Senior Lecturer, is with the Department of Mechanical Engineering, Faculty of Engineering, University of Malaya, and also with the Department of Mechanical Engineering, Faculty of Engineering, Assiut University, Assiut 71516, Egypt.

Manuscript submitted April 10, 2013.

Article published online October 23, 2013

changes at high temperatures, non-uniformity, and improper microstructural control, which may be responsible for irreparable damage in the aviation industry, for one.^[7,8] In recent years, in response to these limitations, the magnetron sputtering technique has been suggested by many researchers.^[12–15]

Baradaran *et al.*^[16] studied the adhesion strength of Ti coating on alumina substrate for biomedical applications. In their study, they have coated pure titanium on alumina using PVD magnetron sputtering. The maximum scratch force value was roughly 1102.63 mN. Sultana *et al.* investigated two different thin-film coating methods in transmission laser micro-joining of thin Ti film-coated glass and polyimide for biomedical applications. The effect of two different thin metal film coating methods was studied in transmission laser micro-joints of titanium-coated glass and polyimide. The coating methods were cathodic arc physical vapor deposition (CA-PVD) and electron beam evaporation (EB-PVD). The adhesion of Ti film on glass *via* CA-PVD was superior to that by the EB-PVD method. This is likely due to a higher film deposition rate and consequently a higher adhesion or sticking coefficient for the CA-PVD particles arriving on the substrate compared to those of the EB-PVD film. CA-PVD produced around 4 times stronger laser joints than EB-PVD, which created a Ti film with poor laser joining properties owing to inferior initial adhesion to the substrate, very smooth surface characteristics, and a propensity for generating hotspots consequent to local film decohesion. On the other hand, CA-PVD yielded a more effective metal film as the deposited film was robust with improved adhesion and a rougher substrate, which had an impact on the enhanced joint strength.^[17]

Throughout the last few decades, pure titanium has most widely been utilized as a metallic material thanks to the favorable mechanical properties, corrosion resistance, and strength for use in load-bearing applications compared to other metals. Nonetheless, the nanostructure morphology of titanium has been increasingly considered by numerous researchers.^[18] Nanostructure properties are mainly dependent on nanostructure morphology.^[19] According to different applications, nanostructured layers are fabricated with varying surface areas and uniform size distributions for suitable performance.^[20–22] Titanium oxide (TiO₂) nanotubes may be fabricated by different means, including hydrothermal, electrodeposition, and anodization.^[19–22] Among these methods, anodization is preferred to other processes because surface adhesion and mechanical integrity are essential for hard coating.

To the best of our knowledge, only few studies have been done on the fabrication of TiO₂ nanotubular arrays on Ti-6Al-4V using the anodizing technique. Macak *et al.*^[23] have worked on self-organized nanotubular oxide layers on Ti-6Al-7Nb and Ti-6Al-4V formed by anodization in NH₄F solutions. The influence of niobium and vanadium on the passivity of titanium-based implants in physiological solution has been assessed by Metikoš-Huković *et al.* In their effort, the effect of niobium and vanadium as alloying elements on titanium alloy passivity was investigated in Hanks'

Balanced Salt Solution (HBSS) at 310 K (37 °C) and pH 6.9. The excellent passivating properties of the anodically formed Ti(IV)-based surface oxide film and high corrosion resistance of Ti6Al6Nb alloy are attributed to the stabilizing effect of Nb (5+) cations on the passive film. This is due to the eradication of stoichiometric defects (anion vacancies) caused by the presence of titanium suboxides.^[24]

The basic mechanical and fatigue properties of titanium alloys used in biomedical applications have been reported earlier.^[3] Therefore, the aim of this research work was to improve the mechanical properties of Ti-6Al-4V, such as surface hardness, coating adhesion, and fretting fatigue life by applying a TiO₂ nanotubular array thin-film coating. For this reason, all samples were coated with pure titanium by the PVD magnetron sputtering technique. Taguchi optimization was carried out to attain higher Ti coating adhesion to the substrate. To create nanotubular TiO₂ (nTi), ammonium fluoride (NH₄F) containing water and ethylene glycol (EG) was anodized at a voltage of 20 V. Further insight into the structure of the coating and titanium nanotubes was gained with FESEM and XRD. The adhesion strength between Ti-6Al-4V and pure Ti was evaluated by a micro-scratch tester. Mechanical indentation including hardness and elastic modulus was measured with a nanoindentation test. The fretting fatigue lives of coated specimens were analyzed using a rotating bending fretting fatigue test machine.

II. SAMPLE PREPARATION AND EXPERIMENTAL PROCEDURE

A. Fretting Fatigue Sample Preparation

Cylindrical test specimens (Figure 1(a)) were machined by lathe turning (CNC LATHE MACHINE, Miyano, BNC-42C5) in accordance with ISO 1143 standard.^[25] Fretting fatigue pads were fabricated from an AISI 4140 steel plate with hardness of 346 HV. The substrate material (310 HV) is softer than the pads, but the TiO₂ coating (570 HV) is harder. The friction pad drawings are depicted in Figure 1(b). To simulate fretting fatigue conditions, bridge-type friction pads and a ring-shaped load cell were designed and constructed. Figure 1(c) presents a schematic view of the fretting fatigue test rig used in this research work.

B. Coating Sample Preparation and Process

The material investigated in the current study is Ti-6Al-4V. All samples (diameter of 20 mm and thickness of 5 mm) were polished with SiC paper of 800 to 2000 grit, after which their surfaces were polished to a mirror finish with diamond liquid. The substrates were ultrasonically cleaned in acetone for 14 minutes, thoroughly rinsed with distilled water, and dried using nitrogen gas to avoid contamination.

The most important experimental design stage when using the Taguchi approach lies in the control parameter selection and identifying the orthogonal array (OA).^[26] This experiment comprised three parameters with three

levels each; thus, the fractional factors design used was a standard L_9 orthogonal array. This particular array was chosen due to its capability to verify the interactions among parameters. The nine experiments performed and the details regarding all combinations of experimental conditions for each control parameter are shown in Table I.

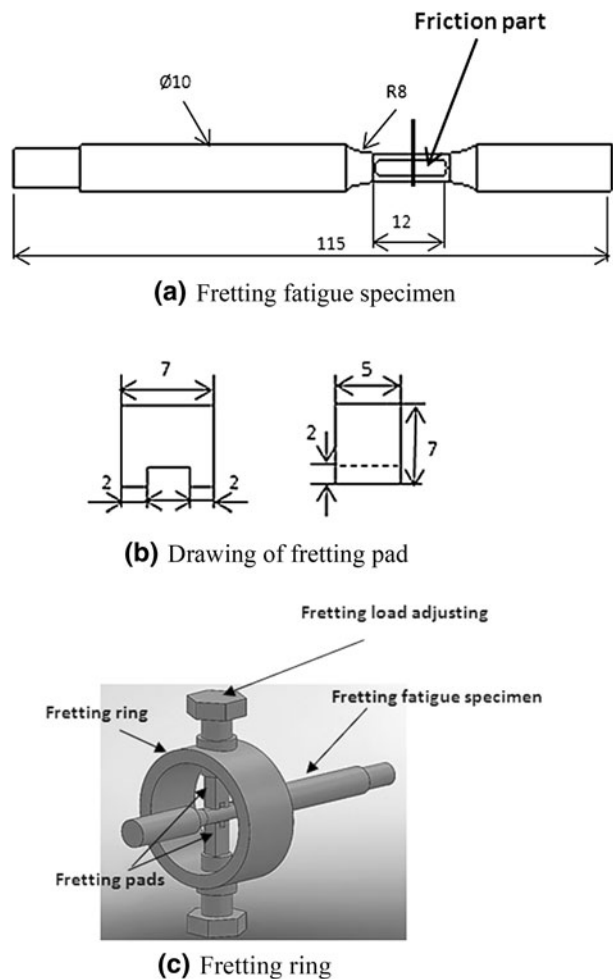


Fig. 1—Drawings of the (a) fretting fatigue specimen, (b) the fretting pad (all dimension are given in mm), and (c) fretting ring.

Table I. Parameters and Levels Used for Experimental Work

Exp.	Factors		
	DF Power (W)	Temperature [K (°C)]	DC Biases Voltage (V)
1	200	426.15 (150)	25
2	200	473.15 (200)	50
3	200	523.15 (250)	75
4	300	426.15 (150)	50
5	300	473.15 (200)	75
6	300	523.15 (250)	25
7	350	426.15 (150)	75
8	350	473.15 (200)	25
9	350	523.15 (250)	50

Thin films of metal were experimentally deposited using a magnetron sputtering system (A SG control engineering Pte Ltd series). A titanium film was deposited on Ti-6Al-4V alloy as a substrate *via* DC magnetron sputtering. A titanium (99.995 pct purity) target with 160 mm diameter was clamped to a planar sputter source that was mounted horizontally on the base of the chamber. The distance between the target and the substrate was maintained at 150 mm. The substrates were cleaned with acetone and ethanol in an ultrasonic bath prior to deposition. The target was pre-sputtered in argon atmosphere to remove the oxide layer. The chamber was evacuated to below 333.305×10^{-5} Pa (2.5×10^{-5} Torr) before the argon gas for sputtering was introduced. The flow of argon gas was fixed at 20 sccm, while the working pressure was kept at 693.274×10^{-3} Pa (5.2×10^{-3} Torr).

C. Sample Preparation for TiO_2 Nanotube Process

The coated samples were anodized in electrolyte containing typical ethylene glycol (EG, J.T. Baker CO.) and water (75:25 V:V) in combination with ammonium fluoride (NH_4F , Sigma-Aldrich CO., 0.5 wt pct) at room temperature (297.15 K (24 °C)). A direct current (DC) power source (Model E3641A, Agilent Technologies, Palo Alto, USA) was used for the process of anodization. The coated sample was connected to the positive terminal of the power source (cathode) and a graphite rod ($D = 5$ mm) was connected to the negative terminal (anode). The distance between the cathode and anode was maintained at about 20 mm. Surface anodization was done at a constant potential of 20 V at anodization times of 20, 60, and 90 minutes. During anodization, the color of titanium as a second layer normally changed from purple to blue and finally light green. Thermal annealing was performed in an argon gas furnace at 753015 K and 923.15 K (480 °C and 650 °C) for 2 hours with heating and cooling rates of 278.15 K min^{-1} (5 °C min^{-1}).

D. Surface Characterization

The coating's morphology was observed through a high resolution FEI Quanta 200F field emission scanning electron microscope (FESEM). A cross section of the coating was also studied by a relatively destructive method. X-Ray diffraction (XRD) patterns of the prepared and annealed samples were recorded on an Empyrean X-Ray diffractometer with $Cu K_\alpha$ radiation ($\lambda = 1.54178$ Å) operating at 45 kV and 30 mA with 0.026-deg step size at the scanning rate of $0.1^\circ s^{-1}$ in a 2θ range from 20 to 80 deg). The coating's mechanical properties were investigated by nanoindentation. A commercial nanoindenter (Micro materials Ltd. Wrexham, U.K.) with continuous stiffness measurement capability was applied. The nanoindentation experiment used a nanoindenter system with a Berkovich diamond tip (20 nm radius and constant dept of 800 nm). The indentation velocity was 3 to 6 nm/s, and once the maximum prescribed depth was reached, loading stopped and the load was maintained constant for

Table II. Measured Adhesion Strength and Calculated (S/N) Ratio

Exp	Scratch Force (mN)				Calculated S/N Ratio
	1st	2st	3st	Ave.	
1	854	887	887	876	58850
2	1295	1301	1262	1286	62185
3	1390	1380	1401	1390	62860
4	1655	1654	1632	1647	64334
5	1159	1114	1282	1185	61474
6	1020	1009	1007	1012	60103
7	2376	2390	2419	2395	67586
8	1553	1574	1556	1561	63868
9	981	952	938	957	59618

10 seconds. Adhesion strength was measured (Micro materials Ltd. Wrexham, U.K.) quantitatively using a micro-scratch tester. A diamond indenter (Rockwell type) with 25 μm radius applied an initial load of zero onto a sample. The sliding velocity was 5 $\mu\text{m/s}$ and the load was increased gradually by 9.2 mN/s.

E. Fretting Fatigue

The fretting fatigue specimens were gripped and loaded rotationally in a rotating bending fretting fatigue test apparatus. By adjusting the load screw on a proving ring with a torque driver, the normal contact load between the contact pads and specimen was controlled. The fretting fatigue tests were carried out at constant average contact pressure of 100 MPa. Average contact pressure was calculated by dividing the contact (normal) load per foot of fretting pad by the apparent contact area. When a fatigue specimen is subjected to cyclic stresses, fretting between the contact pads and specimen is generated. The samples employed in the fretting fatigue test were uncoated and TiO₂-coated Ti-6Al-4V. Plain and fretting fatigue testing took place at room temperature in a two-point loading rotating bending machine ($R = -1$) under constant stress amplitude at a rotational speed of 3000 rpm. The nominal maximum cyclic stress was set at a value that was expected to result in fatigue life between 10⁴ and 10⁷ cycles; the test was stopped if the specimen did not fail at 1×10^7 cycles. The friction force created by normal force and the sliding movement between the specimen and pads, as well as the friction coefficient, was measured using a friction test machine. The obtained friction coefficient between the pads (AISI 4140 steel) and Ti-6Al-4V was roughly 0.607. The friction force can be determined from the relation $F = \mu \cdot P$, where P is the contact load calculated by the ring-shaped load cell (Figure 1(c)) and F is the friction force measured with the friction test machine.

III. RESULTS, ANALYSIS, AND DISCUSSION

A. Adhesion Strength

The most crucial properties of coating are stability and durability because of the long-term use in connecting and

joining parts of fuselage and automobiles.^[27] Regarding applications, it is important to characterize and thereby improve the adhesion strength between coating layers and metallic materials. The adhesion between the coating and a substrate, and the integrity of the substrate/coating interface are always linked to the performance and reliability of any coated device. In this study, a total of nine experiments were carried out to achieve high adhesion strength and consistency. Table II presents a summary of the adhesion test results. Figure 2 illustrates the scratch length and failure point along with a graph of depth and load vs distance during the scratch force test. The failure point and scratch length of the specimen exhibiting low adhesion strength were 856.34 μm and 1500 mN, respectively.

B. Data Analysis for Higher Adhesion Strength

Following the experimental runs, the data obtained were analyzed to optimize the deposition parameters and identify which process parameters are statistically significant. Data analysis was conducted using signal-to-noise (S/N) response analysis. The methods of calculating the S/N ratio are classified into three main categories, depending on whether small, large, or nominal values are required to obtain the best results. In the case of adhesion strength between coatings and substrates, larger values were required. The following equation is used to calculate the S/N ratio (in dB) under conditions in which large ratios yield the best results:

$$S/N = -10 \log \frac{1}{n} \left(\sum \frac{1}{y^2} \right), \quad [1]$$

where y represents the observed data and n is the number of observations. The S/N ratio functions as a performance measurement that can be used to develop processes insensitive to noise factors. The degree of predictable performance of a product or process in the presence of noise factors can be defined from the corresponding S/N ratios. Table II shows the S/N ratio calculated with Eq. [1] for adhesion strength, while Table III provides the S/N response values for the measured data, which are plotted in Figure 3. The desired “the higher the better” criteria imply that the highest S/N reflects the best response, which results in the lowest effects due to noise on machine setup. This

criterion was employed in this study to determine the optimal coating parameters yielding the highest adhesion strength. As observed in Figure 3 and according to the higher (S/N) response base, the DC power, temperature, and DC bias voltage were significant in determining the best adhesion strength. At these levels, a confirmation test was carried out using the best param-

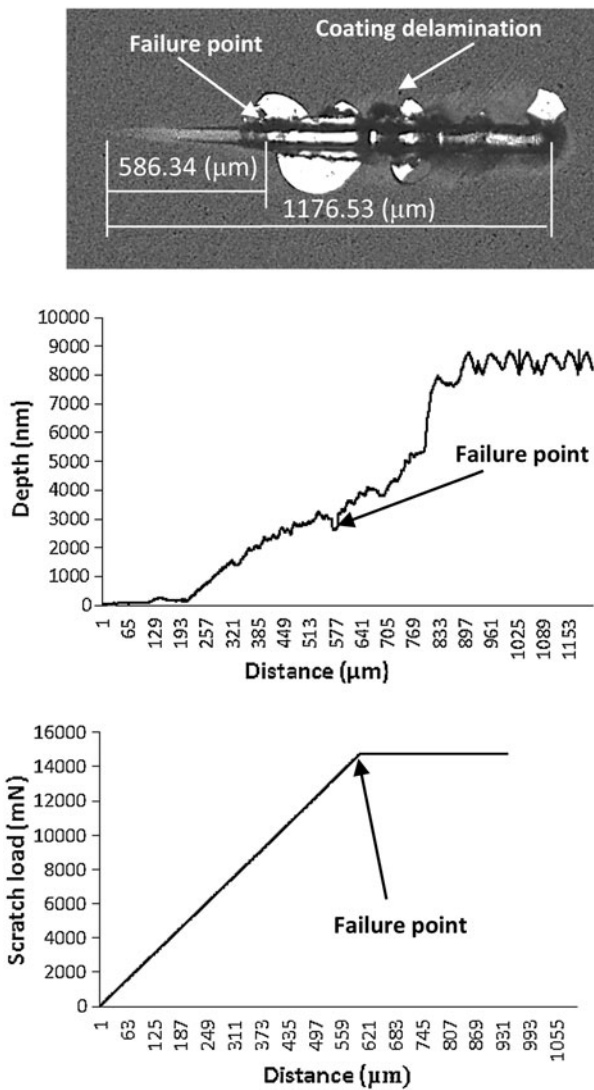


Fig. 2—Scratch adhesion testing on a coated sample and the critical load accompanied by their force and depth vs distance graphs for typically low adhesion at DC power 350W, temperature 473.15 K (200 °C), and DC bias voltage 25 V.

Table III. S/N Response Values for Adhesion Strength (Scratch Force)

Coating Parameters	S/N Response		
	Level 1	Level 2	Level 3
DC power (W)	61.2984	61.971	63.690
Temperature [K (°C)]	63.590	62.509	60.861
DC bias voltage (V)	60.941	61.329	63.973

eter combination to validate the findings. The combination of DC power of 350 W, temperature of 423.15 K (150 °C), and substrate bias voltage of 75 V provided suitable conditions for strong Ti adhesion to Ti-6Al-4V alloy. The results also indicate that a substrate bias voltage of 75 V is more effective in improving coating adhesion. This improvement may be attributed to the additional energy available for film growth. In this case, high-energy atoms with greater mobility settled into lower-energy surface sites, leading to higher coating adhesion and density.^[28] Furthermore, the sputtering rate increased with rising DC power to 350 W because the ionized and sputtered particles became more energized, reducing the distance between the energized atoms and subsequently making the surface more adhesive. Figure 4 presents the scratch length and failure point as well as a graph of depth and load vs distance during the scratch test. It is observed from the graphs that coating has the best adhesion strength. This coated specimen had a scratch length of 1154.37 μm and failure point and load of approximately 976.64 μm and 2545 mN, respectively.

The adhesion strength obtained from this confirmation test was 2545 mN, representing an improvement of 6.27 pct compared with the highest value achieved from the experiments shown in Table II.

C. Microstructure Characterization (Ti Coating and TiO₂ Nanotube Arrays)

Figure 5 illustrates the cross-sectional view of a sample prepared by DC magnetron sputtering (PVD) and the anodised surface on which TiO₂ nanotube arrays were grown as a second layer. The thickness of the Ti/TiO₂ coating was roughly 2.7 μm, where the first and second layers measured approximately 1.554 μm and 1.15 μm thicknesses, respectively. A matte surface was observed on the bottom of the TiO₂ coating. The concave dimples formed at the interface caused an increase in mechanical interlocking and thereby enhanced adhesion strength at the interface.^[29]

Figures 6(a) through (c) show the samples' morphology at various anodization times. As per Figure 6(a), during the first stage of anodization, pore nucleation occurred on the Ti surface due to the pitting corrosion induced by fluoride ions at an anodization time of 20 minutes. In Figure 6(a), it is evident that nanopore

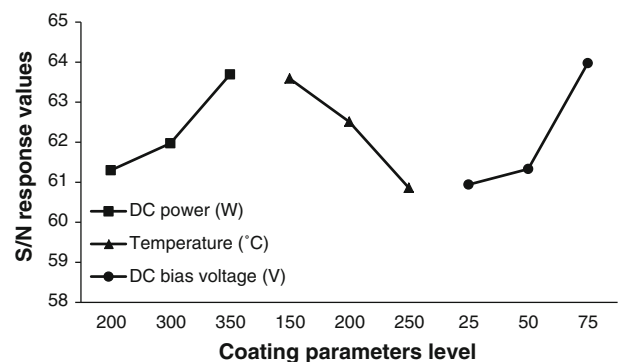


Fig. 3—The S/N response graph for adhesion strength.

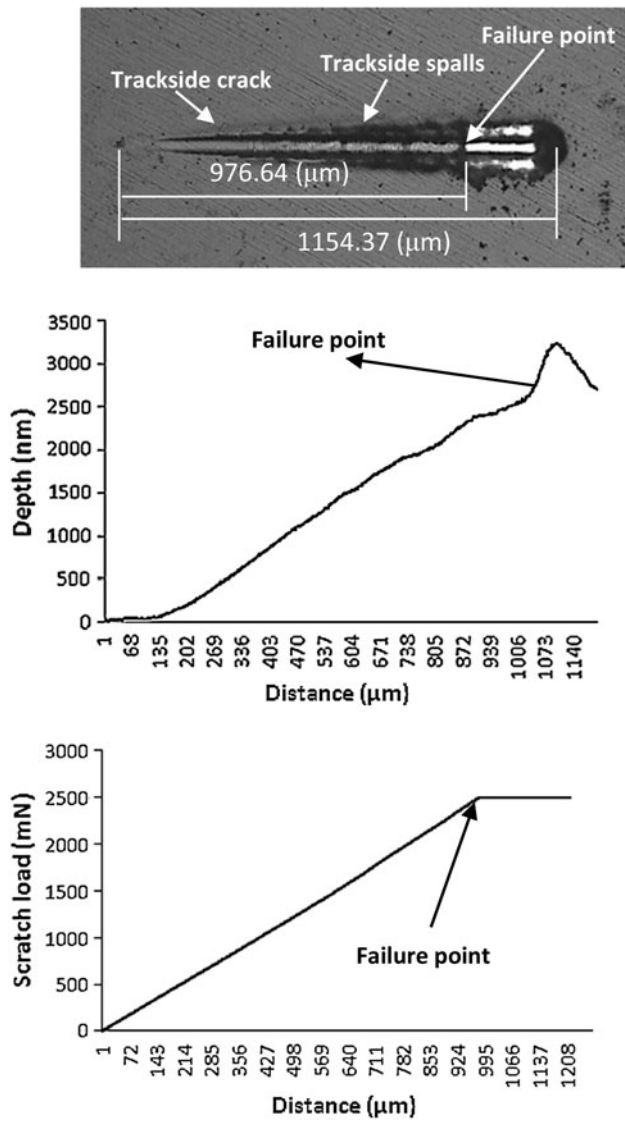


Fig. 4—Scratch adhesion testing on a coated sample and the critical load accompanied by their force and depth vs distance graphs for high adhesion (Confirmation test) at DC power 350 W, temperature 423.15 K (150 °C), and DC bias voltage 75 V.

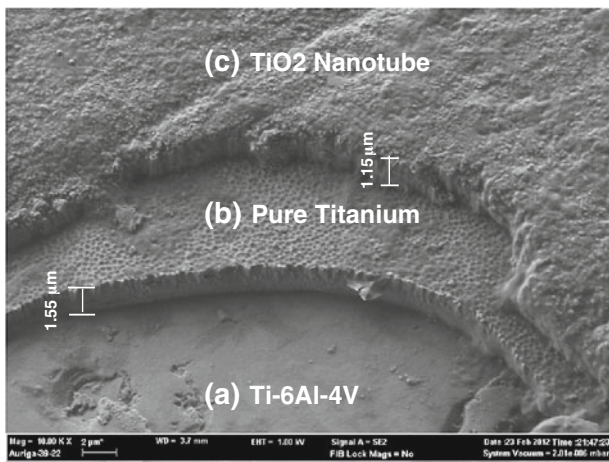


Fig. 5—SEM cross-sectional view (a) Ti-6Al-4V, (b) Pure titanium, and (c) TiO₂ nanotube.

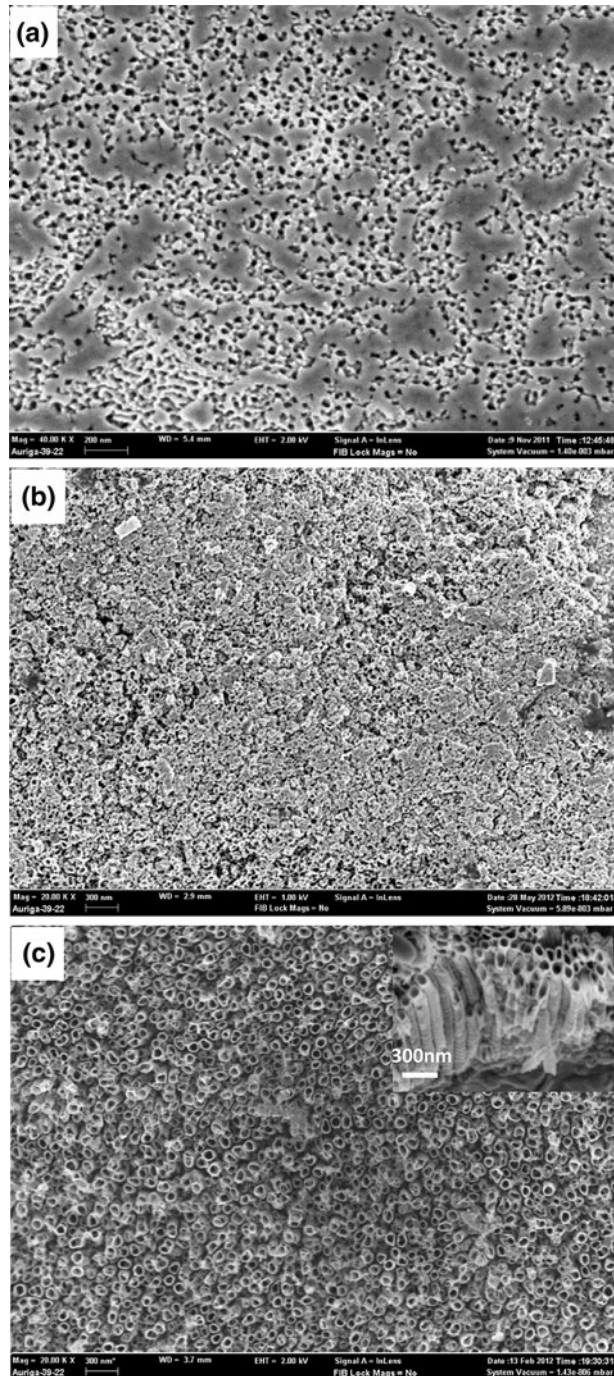


Fig. 6—FESEM top-view images of nanotube array (a) 20 min, (b) 60 min, and (c) 90 min of anodisation.

formation occurred on top of the nanotubes, which were non-homogenous and were poorly organized on the surface with no remaining TiO₂ layer during the first 20 minutes. At an anodization time of 60 minutes (Figure 6(b)), the porous structure was converted to the tubular structure of TiO₂ nanotubes. Figure 6(c) illustrates the top view and cross section of the fractured TiO₂ coating at 90 minutes of anodization. The nanotubes are well defined with an average diameter of approximately 58 nm. The cross section of TiO₂ nano-

tubes indicates a bamboo-shaped structure with good density, which can potentially result in enhanced chemical activity and stronger interactions. It is noteworthy that the coating density is an important factor contributing to good mechanical properties, as will be discussed in the next section.^[9]

D. Crystal Properties

Figure 7 portrays the diffuse diffraction pattern obtained by thin-film X-ray diffraction analysis, where the oxide layer of nanotube arrays formed by electrochemical anodization is crystallized at various annealing temperatures. It is known that the performance of titanium dioxide is highly dependent on the material's phase. In recent years, the anatase and rutile phases have attracted great attention for their high hardness and wear resistance. The rutile phase is more suitable to provide enhanced mechanical properties.^[30] Therefore, the anodized samples were annealed at different temperatures and heating and cooling rate of $278.15 \text{ K min}^{-1}$ ($5 \text{ }^\circ\text{C min}^{-1}$) to obtain rutile phase TiO_2 nanostructures. Figure 7 depicts the XRD patterns of Ti-6Al-4V (a), substrate coated with titanium (b), and the oxide layer of nanotube arrays prepared on a titanium surface annealed at 753.15 K and 923.15 K ($480 \text{ }^\circ\text{C}$ and $650 \text{ }^\circ\text{C}$) for 2 hours in a furnace with N_2 gas (c and d). The peaks for Ti-6Al-4V as the main substrate are clearly detected in Figures 7(b) through (d). The temperature of phase transition from anatase to

rutile is approximately 823.15 K to 923.15 K ($550 \text{ }^\circ\text{C}$ to $650 \text{ }^\circ\text{C}$), as previously reported.^[15,30]

E. Nanomechanical Characteristics

In commercial nanoindenters, the load and displacement are typically recorded continuously during the indentation process, resulting in a load–displacement curve that describes the interaction between the tip and sample throughout the indentation procedure. In recent years, numerous studies on material properties have focused on measuring Young's modulus (E) and indentation hardness (H) from indentation data.^[8,30] Hardness and Young's modulus are parameters that are independent of one another.

This section describes the nanomechanical characterization of titanium oxide nanotube structures on Ti-6Al-4V alloy coated with a pure titanium layer measuring $2.7 \text{ }\mu\text{m}$ in thickness. Figures 8(a) and (b) shows the representative load vs displacement curves for the annealed samples at 753.15 K and 923.15 K ($480 \text{ }^\circ\text{C}$ and $650 \text{ }^\circ\text{C}$), respectively. In general, material properties such as strength and hardness can change as a result of heat treatment at different annealing temperatures. It is important to note that Young's modulus and hardness can be determined instantaneously as a function of depth. Some researchers refer to these as apparent hardness and Young's modulus because of the effect of the substrate on the coatings.^[29] In thin-film nanoinden-

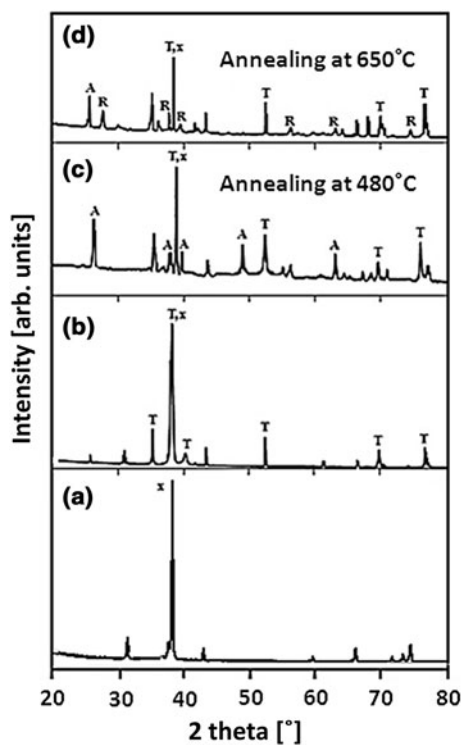


Fig. 7—XRD profiles for (a) Ti-6Al-4V, (b) Ti-6Al-4V/titanium/ TiO_2 nanotube arrays. (c) Sintering at 753.15 K ($480 \text{ }^\circ\text{C}$) and (d) Sintering 923.15 K ($650 \text{ }^\circ\text{C}$) for 2 h (T: titanium coating, x: titanium substrate, A: anatase, R: rutile).

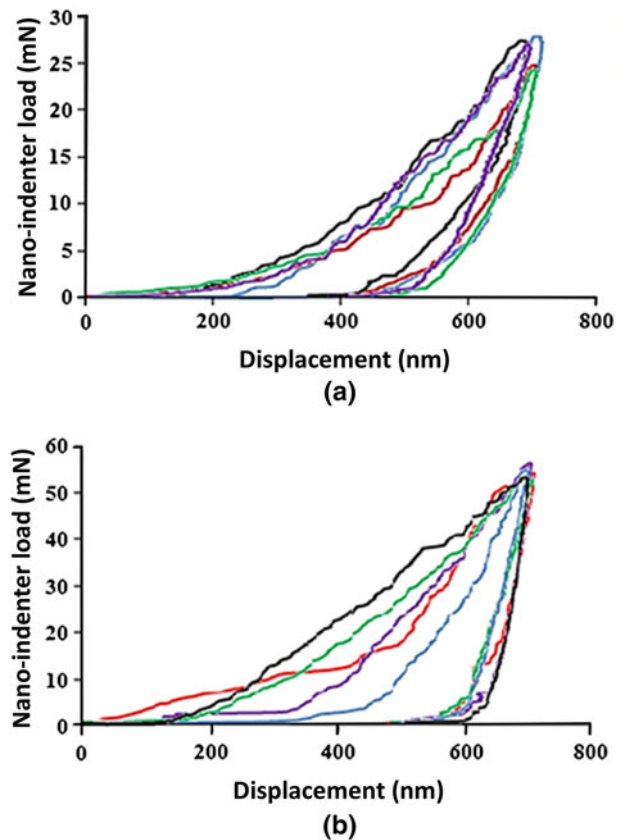


Fig. 8—Characteristic load vs nanoindentation depth for samples anodised at (a) 753.15 K ($480 \text{ }^\circ\text{C}$) and (b) 923.15 K ($650 \text{ }^\circ\text{C}$).

tation, it is common to determine the film's properties at indentation depths of under 10 pct of the film's thickness in order to minimize substrate contributions. It is well known, however, that the modulus of ceramic materials decreases at higher porosities. Several researchers have proposed theoretical models to predict the effect of porosity on the elastic properties of ceramic materials. One of the simplest models is the rule of mixtures, often employed in continuous fiber-reinforced composites. It assumes an isostrain condition (longitudinal loading, parallel to the fibers) or isostress condition (transverse loading, perpendicular to the fibers). In the longitudinal orientation, Young's modulus of the composite, E_c , is given by Eq. [2]:

$$E_c = E_f V_f + E_m V_m; \quad [2]$$

where E and V correspond to Young's modulus and volume fraction, respectively. The subscripts f and m denote fiber and matrix, respectively.^[29] Hashin and Rosen^[31] derived a relationship for a transversely isotropic composite consisting of cylindrical fibers in various aligned packing arrangements. By assuming the "fibers" to be cylindrical pores (*i.e.*, Young's modulus of zero), their equations also reduced to a rule-of-mixtures type of relationship (Eq. [3]):

$$E_c = E_m(1 - P), \quad [3]$$

where E_m is the matrix material and P is the fraction of porosity. In this work, the nanotubes are aligned, as is the porosity between the tubes. Thus, the "rule of mixtures" may be used to determine the Young's modulus of this porous system. For the current analysis, it is observed that the volume fraction of pores in the coating is approximately 70 pct (from image analysis) and a modulus for dense anatase TiO₂ is 190 GPa.^[31] These yield a Young's modulus of anatase TiO₂ nanotubes of approximately 57 GPa.

During the indentation process, nanotube layer densification and the dense surface wear comprised the two main deformation processes that occurred under the indenter tip. This means that the areas under the indenter tip were densified and the other sides of the indenter were subjected to shear stresses that induced both densification and wear. Therefore, as the indenter penetrated the coating surface, the modulus increased due to the increasing contribution of the substrate to the overall layered material strength. In addition, the densification of the area surrounding the indentation slightly contributed to material strength and led to wear between the indenter surface and dense coating surface. As the TiO₂ coating under the indenter became increasingly dense, the modulus increased. Therefore, it was difficult to extract a precise Young's modulus value for the porous coating itself. Moreover, in this study, the maximum depth was fixed at 700 nm with respect to the average nanotube coating's thickness that was 1.15 μm . The maximum load utilized in the nanoindentation test was 60 mN for the TiO₂ nanotube arrays that were developed for an anodization time of 90 minutes at a constant anodization voltage of 20 V. The most common phase transformation of TiO₂ is that from anatase to rutile, of which the rutile is

the more stable phase. According to the results, the films' Young's modulus and hardness increased from 53.81 to 149.36 GPa and from 1.861 to 3.654 GPa, respectively, with annealing temperature, due to the mentioned phase transformation. The elastic modulus data at an annealing temperature of 753.15 K (480 °C) are in close agreement with the Young's modulus values reported by Crawford *et al.* and Shokuhfar *et al.*, who also used nanoindentation.^[30,32] Their reported values ranged from 36 to 43 and 23 to 44 GPa, while for an annealing temperature of 923.15 K (650 °C), the values are quite different from the reported values of approximately 125 to 135 GPa.^[5] Additionally, the hardness values at different annealing temperatures are similar to those reported in previous studies.^[5,6] The values reported by Souza *et al.* were roughly 2 to 3 GPa. A comparison between elastic modulus values of TiO₂ obtained from the nanoindentation test and Eq. [3] indicates that the results are in close agreement, with only 5 pct error. The residual stress (hysteresis loop) during loading and unloading signifies that the nanotube surface undergoes elastic energy dissipation, generating higher stiffness, an elastic response, frictional energy, and compressive plastic deformation. Moreover, the hysteresis loop area increased with annealing temperature. This area represents the energy dissipated due to material plasticity. In general, the surface energy of the anatase phase is lower than that of the rutile phase. The phase transition becomes increasingly apparent at more elevated annealing temperatures.^[30]

F. Fretting Fatigue Test

In order to investigate the fretting fatigue life of Ti/TiO₂-coated specimens, some experiments were carried out and the results are shown in Figures 9 through 11. The experiments were conducted for a stress ratio of $R = -1$, 50 Hz, a constant contact force of 100 MPa, and working stress amplitudes of 150 to 500 MPa. Each data point on the S/N curve represents the average of five specimens tested under identical conditions. Figure 9 includes a comparison of the number of cycles to failure *vs* bending stress for plain fatigue and fretting fatigue of uncoated specimens. It is clear in Figure 9 that the fatigue lives of uncoated specimens diminished with increasing bending stress. Also, fretting had a deleterious effect on fatigue life. To investigate the effects of the rutile phase (annealing) on the fretting fatigue life of coated specimen, Figure 10 provides the comparison between the fretting fatigue life (S/N curve) of uncoated specimens and that of Ti/TiO₂-coated specimens. In Figure 10, it is evident that the fretting fatigue life of Ti/TiO₂-coated specimens with higher surface hardness (4 GPa, rutile phase) improved at low and high cyclic fatigue regimes significantly, which is attributed to the high^[33] surface coating hardness and low friction between the fretting pads and the substrates owing to the presence of the nanotube array.

The effect of the annealing anatase phase on the fretting fatigue life of Ti/TiO₂-coated specimens was additionally investigated. As Figure 11 demonstrates, the fretting fatigue life of coated specimens improved

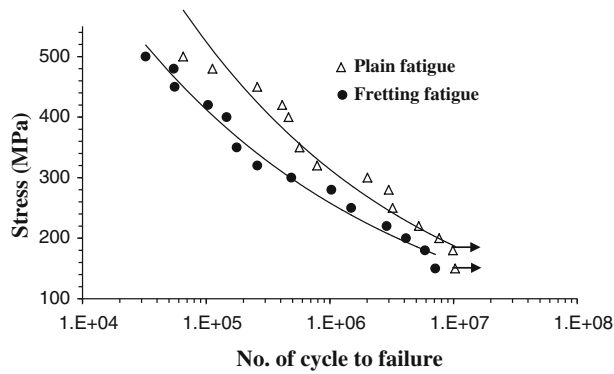


Fig. 9—S/N curve of plain fatigue and fretting fatigue for uncoated specimens.

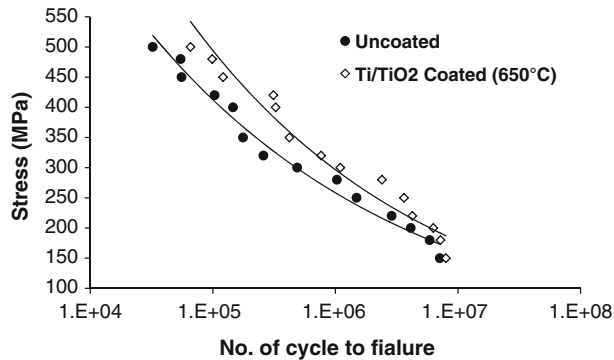


Fig. 10—S/N curve of fretting fatigue for uncoated specimen and Ti/TiO₂-coated specimen with annealing temperature 923.15 K (650 °C).

compared to uncoated specimens in both high and low cyclic fatigue (LCF) due to the high hardness (2.04 GPa) and low coefficient of friction amid friction pads and samples.^[34,35] A comparative study on the S/N curves of coated specimens with various heat treatment temperatures (rutile and anatase phases) indicates that the annealing temperature of 480, which causes the generation of an anatase phase, has a better effect on the fretting fatigue life of coated Ti-6Al-4V at high cyclic fatigue than coated specimens with higher hardness (4 GPa, rutile phase). This phenomenon is potentially attributed to the ceramic nature and brittleness of TiO₂ nanotubes with greater hardness (4 GPa).^[33,36] Cracks initiate in contact areas (fretting pads and TiO₂ nanotube coating) because of high stress concentration, and with continuous cyclic load the cracks propagate toward the titanium coating. Since the Ti coating to substrate adhesion is strong and Ti also penetrates the substrate (PVD magnetron sputtering technique nature), cracks transfer and propagate to the substrate.^[10,11,37,38]

For further analysis, an SEM micrograph test was carried out. Figure 12 illustrates the crack propagation and fracture of uncoated specimens with higher magnification at a bending stress of 300 MPa and 2E10⁶ cycles. The crack started in the contact area (substrate and contact pressure of fretting ring) and propagated inside the substrate. Furthermore, the fractures of Ti/TiO₂-

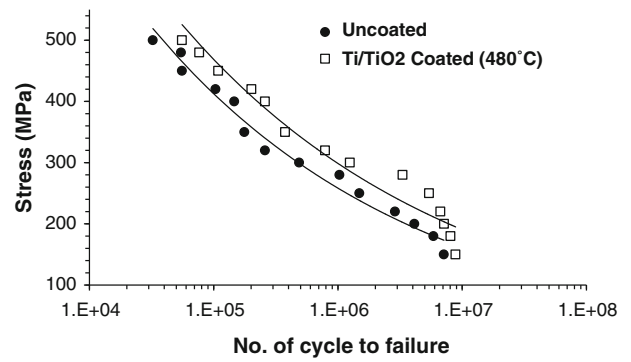


Fig. 11—S/N curve of fretting fatigue for uncoated specimen and Ti/TiO₂-coated specimen with annealing temperature 753.15 K (480 °C).

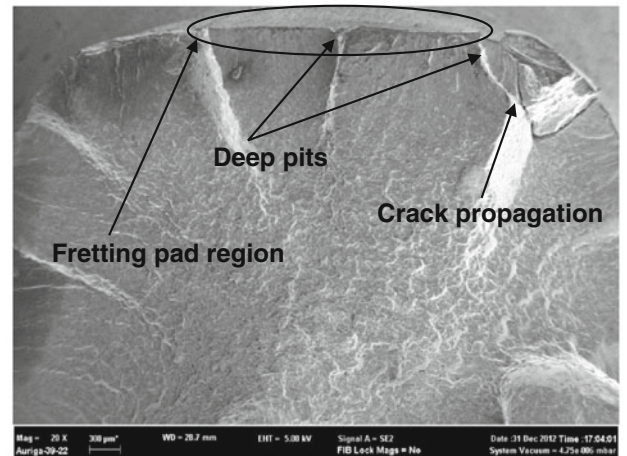
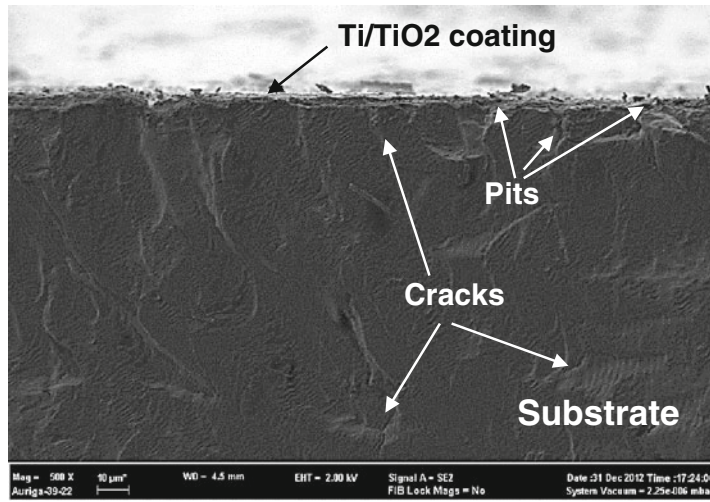
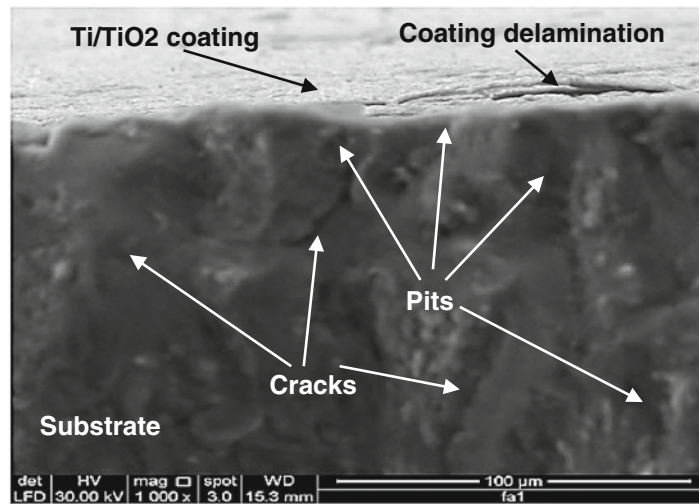


Fig. 12—Crack propagation and fracture of uncoated specimen under fretting fatigue at bending stress 300 MPa and 2E10⁶ cycles.

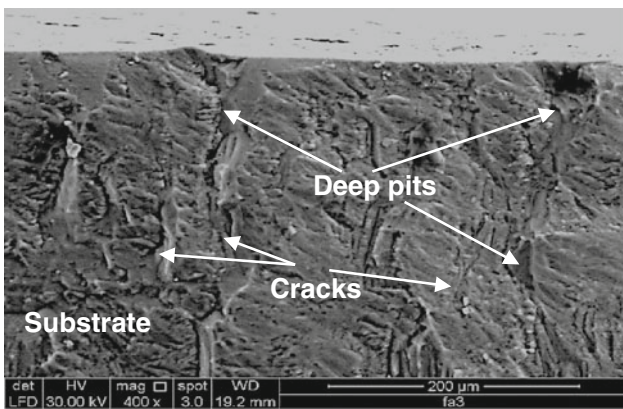
coated specimens at an annealing temperature of 923.15 K (650 °C, rutile phase), and different bending stresses and cycles are presented in Figure 13. Figure 13(a) shows the Ti/TiO₂-coated specimen fracture at 350 MPa bending stress and 4.2E10⁵ cycles. A number of cracks and pits inside the substrate and Ti/TiO₂ thin-film coating are visible under SEM, which resulted from the fretting pads and fretting fatigue. Figure 13(b) presents the Ti/TiO₂-coated specimen fracture at 250 MPa bending stress and 3.6E10⁶ cycles. Clearly, the coating delaminated from the substrate as a consequence of the contact pressure of the fretting fatigue pads. At 180 MPa bending stress, and around 7.1E10⁶ fatigue cycles, a few parts of Ti/TiO₂ coating still remained on the fretting fatigue specimen's surface (see Figure 13(c)). At a lower bending stress (150 MPa) and higher number of cycles (around 7.9E10⁶) as shown in Figure 13(d), the coating totally detached under the edge of the fretting pads. This implies that brittleness of the Ti/TiO₂ hard coating was responsible for the coating removal.^[2,40] In addition, it should be explained that nanotube array TiO₂ produced by the anodizing process is part of pure titanium coating; therefore, the adhesion is greater compared to that between titanium and substrate. Hence,



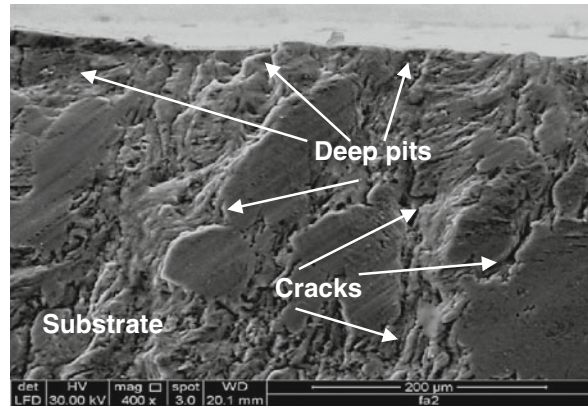
(a)



(b)



(c)



(d)

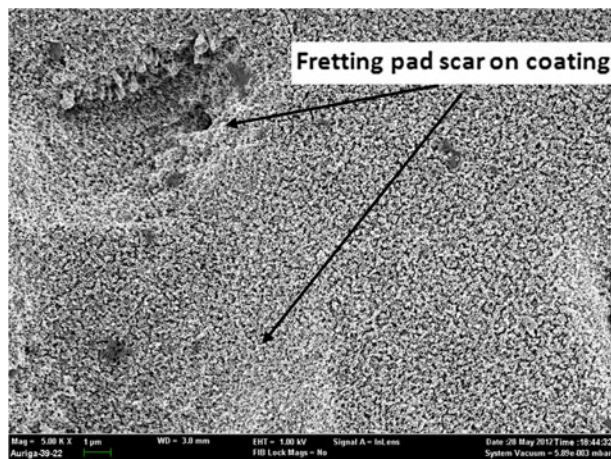
Fig. 13—Fracture of Ti/TiO₂-coated specimens with annealing temperature 923.15 (650 °C) (rutile phase) under fretting fatigue at different bending stresses and cycles. (a) At bending stress 350 MPa and 4.2E10⁵ cycles, (b) at bending stress 250 MPa and 3.6E10⁶ cycles, (c) at bending stress 180 MPa and 7.1E10⁶ cycles, and at bending stress 150 MPa and 7.9E10⁶ cycles.

heat-treated nanotubes at an annealing temperature of 923.15 K (650 °C, which are now ceramics) cracked and detached under the fretting pad pressure. Due to their

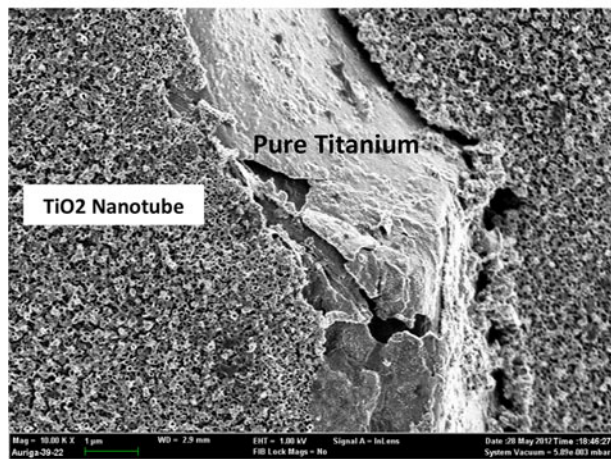
high adhesion, they delaminated from the substrate's surface, and thus with further continuation in cyclic load the coating was gradually removed.^[39]

Figures 14(a) and (b) present SEM micrographs of the Ti/TiO₂ coating surface at an annealing temperature of 923 K (650 °C, rutile phase) under the fretting pad (100 MPa). It is obvious in Figure 14(a) that there are scars on the coating (Ti/TiO₂) at a bending stress of 400 MPa and 3.2E10⁵ cycles. From this image, it can be understood that the coating is sufficiently hard to tolerate the fretting fatigue pads (Rutile phase).^[32,33,40] Figure 14(b) shows the crashed and detached coating (titanium and TiO₂) at a bending stress of 180 MPa and 7.1E10⁶ cycles as a result of the friction pad. Besides, by increasing the cyclic load up to roughly 7.1E10⁶, the coating cracked, crashed, and detached from the substrate which is due to the ceramic nature and brittleness of TiO₂ coating. Furthermore, Figures 14(a) and (b) also supports Figures 12(a) and (b).

Figures 15(a) and (b) depict Ti/TiO₂-coated specimen fracture at an annealing temperature of 753.15 K (480 °C, anatase phase), bending stress of 300 MPa and 1.2E10⁶ cycles, and with 180 MPa bending stress



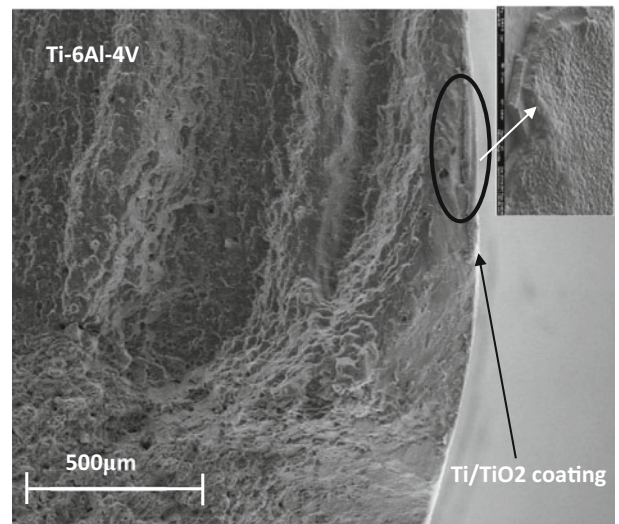
(a)



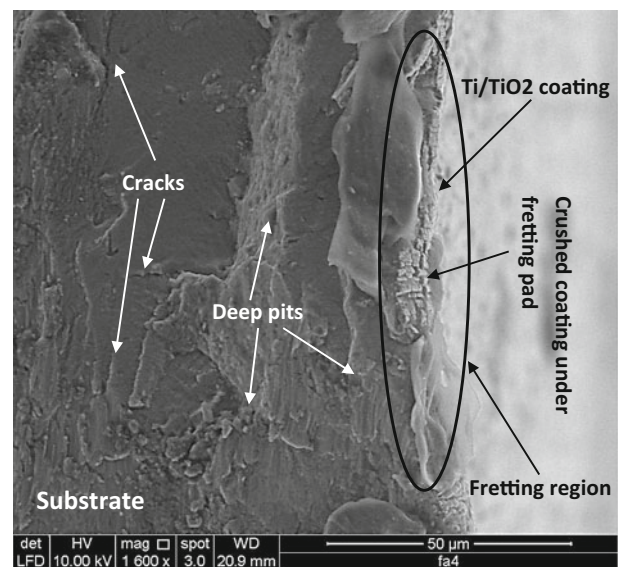
(b)

Fig. 14—SEM micrograph of the scars and crack propagation on the surface of Ti/TiO₂-coated specimen with annealing temperature 923.15 K (650 °C, rutile phase) under fretting pad (100 MPa) at bending stress (a) 400 MPa and 3.2E10⁵ cycles and (b) 180 MPa and 7.1E10⁶.

and 8E10⁶ cycles, respectively. Cracks and pits are visible in the fracture fretting fatigue specimens. A study of these images suggests that some Ti/TiO₂ coating still remained under the fretting pads at high cyclic load (8E10⁶ cycles). This is attributed to the compressibility properties of TiO₂ nanotube coating that was heat treated at an annealing temperature of 753.15 K (480 °C, anatase phase) under friction pads, thus making the coating tolerate even higher cyclic loads.^[33,34,39–42] Figures 16(a) and (b) shows the crushed Ti/TiO₂ nanotube coating under fretting pads (100 MPa) at a bending stress of 300 MPa and 1.2E10⁶ cycles, and 180 MPa and 8E10⁶ cycles, respectively, therefore showing good agreement with this result (Figures 15(a) and (b)).

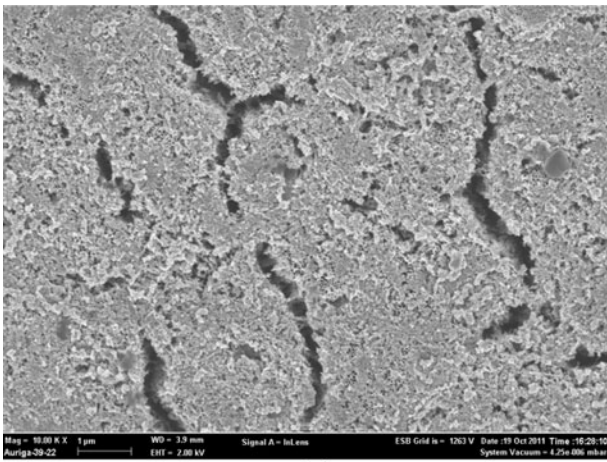


(a)

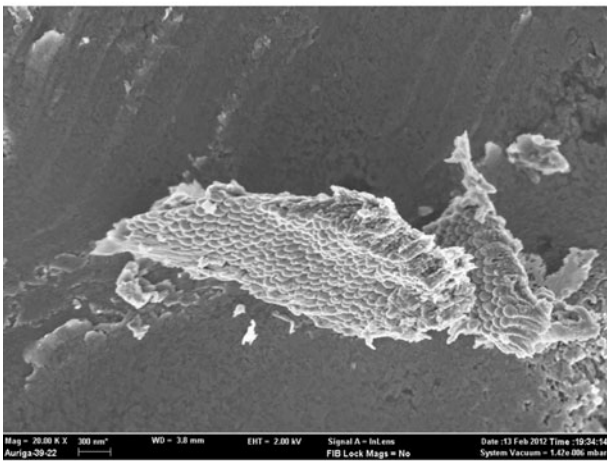


(b)

Fig. 15—Fracture of Ti/TiO₂-coated specimen with annealing temperature 753.15 K (480 °C, anatase phase) at bending stress (a) 300 MPa and 1.2E10⁶ and (b) 180 MPa and 8E10⁶.



(a)



(b)

Fig. 16—The crushed Ti/TiO₂ nanotube coating under fretting pad (150 MPa) at bending stress (a) 300 MPa and 1.2E10⁶ cycles and (b) 180 MPa and 8E10⁶ cycles.

IV. CONCLUSIONS

In this research work, pure titanium was successfully applied as a first layer coat onto Ti-6Al-4V alloy by the PVD magnetron sputtering technique. Taguchi optimization with the orthogonal array L9 was used to obtain the most optimum parameters for the best surface adhesion. The parameters in this study include DC power, temperature, and DC bias voltage. The strong surface adhesion was obtained at DC power of 350 W, temperature of 423.15 K (150 °C), and substrate bias voltage of 75 V. The film exhibiting the strongest adhesion had a scratch length of 1154.37 μm, failure point of approximately 976.64 μm, and load of 2545 mN. TiO₂ nanotubes were synthesized as a second layer by electrochemical oxidation using a mixture of NH₄F, glycerol, and water as an electrolyte. The FESEM results indicate that the best anodization time, *i.e.*, that allowing for the most suitable nanotube formation, was 90 minutes. The phase transition temperature for the anatase phase to rutile phase transformation ranged from 753.15 K to 923.15 K (480 °C to 650 °C). Nanohardness measurements were made with a

nanindentation machine. The results of mechanical indentation tests indicate that Young's modulus and hardness increased with annealing temperature up to 149.36 and 3.654 GPa, respectively. Moreover, the fretting fatigue life of uncoated and Ti/TiO₂-coated specimens was investigated. According to the results, the fretting fatigue life of Ti/TiO₂-coated samples that were heat treated at annealing temperatures of 753.15 K (480 °C, anatase phase) and 923.15 K (650 °C, rutile phase) was enhanced at high cyclic fatigue and low cyclic fatigue compared to uncoated specimens. However, the S/N curves show that Ti/TiO₂ coating on Ti-6Al-4V alloy with heat treatment at an annealing temperature of 753.15 K (480 °C) is more appropriate for higher cyclic load rather than low cyclic load. Besides, Ti/TiO₂ coating on Ti-6Al-4V alloy with heat treatment at an annealing temperature of 923.15 K (650 °C) is more suitable for low cyclic load (high bending stress).

ACKNOWLEDGMENTS

The authors acknowledge the financial support under the Research Grant with No.: UM. TNC2/IPPP/UPGP/261/15 (BK030-2013) from the University of Malaya, Malaysia.

REFERENCES

1. M. Niinomi: *Metall. Mater. Trans A*, 2001, vol. 32A, pp. 477–86.
2. M. Niinomi: *Mater. Trans.*, 2008, vol. 49 (10), pp. 2170–78.
3. M. Niinomi: *Biomaterials*, 2003, vol. 24, pp. 2673–83.
4. A.P. Tomsia, E. Saiz, J. Song, and C.R. Bertozzi: *Adv. Eng. Mater.*, 2005, vol. 7 (11), pp. 999–1004.
5. G.B. de Souza, G.G. de Lima, N.K. Kuromoto, P. Soares, C.M. Lepienski, C.E. Foerster, and A. Mikowski: *J. Mech. Behav. Biomed. Mater.*, 2011, vol. 4 (5), pp. 796–806.
6. G.B. de Souza, C.M. Lepienski, C.E. Foerster, N.K. Kuromoto, P. Soares, and H.A. Ponte: *J. Mech. Behav. Biomed. Mater.*, 2011, vol. 4 (5), pp. 756–65.
7. S.J. Ding, C.P. Ju, and J.H.C. Lin: *J. Biomed. Mater. Res. A*, 1999, vol. 47 (4), pp. 551–63.
8. D.M. Ebenstein and L.A. Pruitt: *Nano Today*, 2006, vol. 1 (3), pp. 26–33.
9. X. Fan, Y. Zhang, P. Xiao, F. Hu, and H. Zhang: *J. Chem. Phys.*, 2007, vol. 20, pp. 753–58.
10. M. Farooq and Z.H. Lee: *J. Korean Phys. Soc.*, 2002, vol. 40 (3), pp. 511–15.
11. S. Gangopadhyay, R. Acharya, A.K. Chattopadhyay, and S. Paul: *Vacuum*, 2010, vol. 84 (6), pp. 843–50.
12. A. Kar, K. Raja, and M. Misra: *Surf. Coat. Technol.*, 2006, vol. 201 (6), pp. 3723–31.
13. P. Kelly and R. Arnell: *Vacuum*, 2000, vol. 56 (3), pp. 159–72.
14. A. Kodama, S. Bauer, A. Komatsu, H. Asoh, S. Ono, and P. Schmuki: *Acta Biomater.*, 2009, vol. 5 (6), pp. 2322–30.
15. K.S. Lee and I.S. Park: *Scripta Mater.*, 2003, vol. 48 (6), pp. 659–63.
16. S. Baradaranan, W.J. Basirun, E. Zalnezhad, M. Hamdi, A.A.D. Sarhan, and Y. Alias: *J. Mech. Behav. Biomed.*, 2013, vol. 20, pp. 272–82.
17. T. Sultana, G.L. Georgiev, R.J. Baird, G.W. Auner, G. Newaz, R. Patwa, and H.J. Herfurth: *J. Mech. Behav. Biomed.*, 2009, vol. 2, pp. 237–42.
18. S. Li, J. Yin, and G. Zhang: *Sci. China*, 2010, vol. 53 (5), pp. 1068–73.

19. S.Q. Liu: *Bioregenerative Engineering: Principles and Applications*, Wiley, Hoboken, NJ, 2007.
20. J. Macak, H. Hildebrand, U. Marten-Jahns, and P. Schmuki: *J. Electroanal. Chem.*, 2008, vol. 621 (2), pp. 254–66.
21. M. Mayo, R. Siegel, A. Narayanasamy, and W. Nix: *J. Mater. Res.*, 1990, vol. 5 (5), pp. 1073–82.
22. V. Nelea, C. Morosanu, M. Iliescu, and I. Mihailescu: *Surf. Coat. Technol.*, 2003, vol. 173 (2), pp. 315–22.
23. J.M. Macák, H. Tsuchiya, A. Ghicov, and P. Schmuki: *Electrochem. Commun.*, 2005, vol. 7 (11), pp. 1133–37.
24. M. Metikoš-Hukovič, A. Kwokal, and J. Piljac: *Biomaterials*, 2003, vol. 24, pp. 3765–75.
25. ISO Standard: Metallic Materials—Rotating Bar Bending Fatigue Testing, ISO International, 2010.
26. J.A. Ghani, I.A. Choudhury, and H.H. Hassan: *J. Mater. Process. Technol.*, 2004, vol. 145 (1), pp. 84–92.
27. J.A. Toque, M.K. Herliansyah, M. Hamdi, A. Ide-Ektessabi, and I. Sopyan: *J. Mech. Behav. Biomed. Mater.*, 2010, vol. 3 (4), pp. 324–30.
28. K. Singh, N. Krishnamurthy, and A.K. Suri: *Tribol. Int.*, 2012, vol. 50, pp. 16–25.
29. G. Crawford, N. Chawla, and J. Houston: *J. Mech. Behav. Biomed. Mater.*, 2009, vol. 2 (6), pp. 580–87.
30. Z. Hashin and B.W. Rosen: *J. Appl. Mech.*, 1964, vol. 31, pp. 223–32.
31. Y. Al-Khatatbeh, K.K.M. Lee, and B. Kiefer: *J. Phys. Chem. C*, 2012, vol. 116, pp. 21635–39.
32. W.Y. Chang, T.H. Fang, Z.W. Chiu, Y.J. Hsiao, and L.W. Ji: *Microporous Mesoporous Mater.*, 2011, vol. 145 (1), pp. 87–92.
33. A. Sadeghzadeh Attar, M. Sasani Ghamsari, F. Hajiesmaeilbaigi, S. Mirdamadi, K. Katagiri, and K. Koumoto: *J. Mater. Sci.*, 2008, vol. 43 (17), pp. 5924–29.
34. M.R. VanLandingham: *J. Res. Natl Inst. Stand. Technol.*, 2003, vol. 108 (4), pp. 249–65.
35. T. Shokuhfar, G.K. Arumugam, P.A. Heiden, R.S. Yassar, and C. Friedrich: *ACS Nano.*, 2009, vol. 3 (10), pp. 3098–3102.
36. B. Rajasekaran, S. Ganesh Sundara Raman, L. Rama Krishna, S.V. Joshi, and G. Sundararajan: *Surf. Coat. Technol.*, 2008, vol. 202 (8), pp. 1462–69.
37. Y. Sun, K. Yan, G. Wang, W. Guo, and T. Ma: *J. Phys. Chem. C*, 2011, vol. 115, pp. 12844–49.
38. G. Majzoobi and M. Jaleh: *Mater. Sci. Eng. A*, 2007, vol. 452, pp. 673–81.
39. X. Zhang and D. Liu: *Trans. Nonferrous Mater. Soc. China*, 2009, vol. 19 (3), p. 557.
40. L. Pazos, P. Corengia, and H. Svoboda: *J. Mech. Behav. Biomed. Mater.*, 2010, vol. 3 (6), pp. 416–24.
41. E. Zalnezhad, A.A.D. Sarhan, and M. Hamdi: *Int. J. Precision Eng. Manuf.*, 2012, vol. 13, pp. 1453–59.
42. A. Vadiraj and M. Kamaraj: *Tribol. Int.*, 2007, vol. 40 (1), pp. 82–88.